Ab initio calculation of thermal expansion with application to understanding Invar behavior in gum metal

I. S. Winter,[1,2,*] J. Montoya,[2] K. A. Persson,[1,2] and D. C. Chrzan[1,3,†]

[1]*Department of Materials Science and Engineering, University of California, Berkeley, California 94720, USA*
[2]*Energy Technologies Area, Lawrence Berkeley National Laboratory, Berkeley, California, 94720, USA*
[3]*Materials Sciences Division, Lawrence Berkeley National Laboratory, Berkeley, California, 94720, USA*

(Received 10 April 2018; published 2 July 2018)

A theoretical examination of the thermal expansion behavior of a variety of metals is conducted using a combination of nonlinear elasticity theory and first-principles calculations that is suitable for high throughput computation. Results of this method show good agreement with experimental values. This method is then used to better understand the low thermal expansion behavior of gum metal by comparing the thermal expansion tensor of Ti_3Nb austenitic (β) and martensitic (α'') gum metal approximants. The thermal expansion coefficient of β is found to be in agreement with experimental results for that of annealed gum metal. The thermal expansion tensor of the α'' phase is shown to be highly anisotropic and exhibit negative thermal expansion along $\langle 110\rangle_\beta$. It is demonstrated that the thermal expansion of the two-phase system, $\beta + \alpha''$, can be estimated using the rule of mixing. By applying this averaging scheme and allowing a texturing along $\langle 110\rangle\{001\}_\beta$ in tandem with the growth of the α'' phase, values for the thermal expansion similar to that seen in cold-rolled gum metal are calculated.

DOI: 10.1103/PhysRevMaterials.2.073601

I. INTRODUCTION

An understanding of the thermal expansion behavior of a material is essential for any engineering application over a range of temperatures. Thermal expansion is also of note from a basic scientific perspective, as it arises from anharmonic phonon contributions to the free energy [1]. In addition, the fact that thermal expansion can be derived from the lattice dynamics of a crystal means that the tensor can be directly calculated from first principles. The framework for one such approach relies on the work of Brugger and Thurston [2,3], who showed that the Grüneisen tensor, and by extension the thermal expansion tensor (with the application of the Debye model [4]) could be directly derived from the second- and third-order elastic constants (SOEC and TOEC).

The fact that this approach relies on elasticity theory is especially intriguing considering recent work by the Materials Project related to the development of workflows for the high-throughput computation of SOEC [5] using density-functional theory (DFT). This, combined with the ability to accurately calculate the TOEC of a crystal of arbitrary symmetry [6], offers the prospect of a path towards the high-throughput calculation of the thermal expansion tensor. One such application of this work could be in the search for materials with extreme thermal expansion behavior.

Metals with a low thermal expansion coefficient (known as Invar) have been known to exist since 1896 [7]. In the initial materials studied, the Invar behavior was attributed to a second-order magnetic transformation between a paramagnetic and (anti-) ferromagnetic state. More recent investigations found that Invar behavior can be induced in shape-memory alloy systems such as Cu-Zn-Al, Ni-Ti, and Cu-Mn-Al [8]. The low thermal expansion tensor in these materials was found to be a result of a martensitic transformation. In addition, cold-rolling the material was shown to dramatically enlarge the temperature range between martensitic start (Ms) and martensitic finish temperatures (Mf) as well as the austenitic start (As) and finish temperatures (Af), and as a result increase the temperature range of Invar behavior.

Invar behavior has been observed in gum metal, a class of Ti-Nb based alloys, as well. Along with a low thermal expansion coefficient, gum metal displays numerous other anomalous properties such as high ductility, a near absence of work-hardening, Elinvar behavior (near constant elastic modulus with respect to temperature), superelasticity, as well as an ultrahigh strength [9]. Gum metal's high strength has attracted much interest due to the possibility of the material's plasticity being governed by the ideal shear strength [10–14]. Relatively little work, however, has concentrated on the origins of Invar behavior in gum metal.

In the original paper on gum metal it was found that Invar behavior was only observed after cold-working the material (as in the case of Al-Cu-Zn [8]), in which case the thermal expansion coefficient was reduced from 8×10^{-6} to $2 \times 10^{-6}\ K^{-1}$ and remained stable from 77 K to approximately 500 K after which the thermal expansion coefficient increased dramatically [9]. It was claimed that the low thermal expansion coefficient was not a result of any phase transformation. However, no other explanation was given for the anomalously low thermal expansion. Kim *et al.* found similar dramatic reductions in the thermal expansion in gum metal [15], but found behavior similar to that of Invar-like shape memory alloys. Cold-rolling the material resulted in a negative thermal expansion in the rolling direction (RD), but showed no change

*Corresponding author: ian.winter@berkeley.edu
†Corresponding author: dcchrzan@berkeley.edu

in the directions transverse to rolling (TD). This anisotropy in thermal expansion was accompanied by a large ⟨110⟩{001} texture in RD. In addition, Martensitic-like nanodomains were seen in the same orientation as the texture.

Perhaps the simplest method to calculate the thermal expansion of a crystal is by use of the quasiharmonic approximation [16]. However, this method relies on the fact that the material is dynamically stable at 0 K. This is not the case for many BCC metals that are only stable at high temperature, e.g., Ti_3Nb [17]. As a result, another method is needed to calculate the thermal expansion coefficient. In the case of a Ti_3Nb approximation of gum metal, the G1 structure, the crystal is elastically stable at absolute zero, but dynamically unstable, which is driven by a soft optical phonon mode [17]. Optical phonons, in the harmonic approximation, are related to atomic vibration within a unit cell, but not distortion of the cell itself. Accordingly, the present approach approximates thermal expansion by estimating the strain dependence of acoustic phonons using nonlinear elasticity theory and ignoring the optical phonon contribution to the free energy.

In this paper, we show that by accurately calculating the second- and third-order elastic constants the thermal expansion tensor can be obtained for a range of materials. We then apply this method to the β and α'' phases of gum metal with the goal of explaining the origin of Invar behavior in the material. Further, we demonstrate that, due to the small difference in second-order elastic constants between the two phases of gum metal, by applying the rule of mixing to the thermal expansion tensors, the $\beta + \alpha''$ composite exhibits values similar to those found by Kim *et al.* after cold-rolling gum metal [15], thus supporting the finding that the anomalous thermal expansion of gum metal is related to a texturing effect as well as a phase transformation to α'', but not necessarily invalidating the possibility of Invar behavior occurring without a martensitic phase transformation.

II. METHOD

The derivation of the thermal expansion tensor in terms of the elastic constants begins by relating the thermodynamic Grüneisen parameter to thermal expansion. Using pressure-volume variables the thermodynamic Grüneisen parameter expresses the change in pressure with respect to internal energy [18] at constant volume

$$\gamma = V\left[\frac{\partial P}{\partial U}\right]_V. \tag{1}$$

Using Maxwell relations γ can be expressed in terms of the thermal expansion (α), the isothermal bulk modulus (K), and the constant-volume heat capacity (C_V), as

$$\gamma = V\frac{\alpha K}{C_V}. \tag{2}$$

Substituting stress-strain variables for pressure-volume variables the thermal expansion tensor can be represented in terms of the compliance tensor (S_{ijkm}), constant-strain heat capacity (C_η), and thermodynamic Grüneisen tensor (TGT) (Einstein summation is implied for all roman subscripts):

$$\alpha_{ij} = \frac{C_\eta}{V} S_{ijkm}\gamma_{km}, \tag{3a}$$

$$\gamma_{km} = V\left[\frac{\partial \sigma_{km}}{\partial U}\right]_V. \tag{3b}$$

It is now necessary to relate the TGT to the generalized Grüneisen tensor (GGT). The relation between the GGT and the elastic constants is based on the work of Brugger and Thurston [2,3]. Specifically, the GGT is related to the change in vibrational frequency at a particular wave vector $[\omega_\beta(\boldsymbol{q})]$ with respect to the Lagrangian strain tensor (η_{ij}) by

$$\gamma_{ij}^{\beta}(\boldsymbol{q}) = -\frac{1}{\omega_\beta(\boldsymbol{q})}\left[\frac{\partial \omega_\beta(\boldsymbol{q})}{\partial \eta_{ij}}\right]_{\boldsymbol{\eta}'}. \tag{4}$$

In the above equation, β refers to the polarization index ($\beta = 1,2,3$) and $\boldsymbol{q}$ is the wave vector. If values of $\boldsymbol{q}$ only in the long-wavelength limit are considered, the frequency can be shown to depend only on the direction of the wave vector, leading to Eq. (4) being rewritten in terms of the unit wave vector $\boldsymbol{N}$ in the $\boldsymbol{q}$ direction. In solving for the GGT, it is helpful to define three coordinates: $\boldsymbol{a}$, the coordinate in the unstressed or "natural" state; $\boldsymbol{X}$, the coordinate in the reference stressed state; and $\boldsymbol{x}$, the coordinate in the current, stressed state. The long-wavelength limit allows for the displacement ($\boldsymbol{u} = \boldsymbol{x} - \boldsymbol{X}$) to be written as a plane wave of the form

$$u_j = A_j e^{i\omega\left(t - \frac{N_k a_k}{W}\right)}, \tag{5}$$

where W is the natural wave velocity, t corresponds to time and $\boldsymbol{A}$ is an eigenvector. The natural wave velocity can be related to the vibrational frequency by substituting the right side of Eq. (5) into the equation of motion for an elastic continuum,

$$\rho_0 \frac{d^2 u_j}{dt^2} = \frac{\partial \tilde{P}_{jp}}{\partial a_p}, \tag{6}$$

with $\tilde{P}_{jp}$ being the first Piola-Kirchhoff stress tensor relating the configurations $\boldsymbol{x}$ and $\boldsymbol{a}$, and ρ_0 being the density of the undeformed material. Writing $\tilde{P}_{jp}$ as a Taylor series expansion with respect to the deformation gradient [3] (see Sec. A for derivation) and combining Eqs. (5) and (6) results in an eigenvalue problem, known as the Christoffel equation, of the form

$$\rho_0 W^2 U_j = \Gamma_{jk} U_k, \tag{7a}$$

$$\Gamma_{jk} = N_p[\delta_{jk} t_{pm} + (\delta_{qk} + 2\eta_{qk}) C_{pjqm}]N_m, \tag{7b}$$

with t_{pm} being the second Piola-Kirchhoff stress tensor at $\boldsymbol{X}$ and $\boldsymbol{U}$ being an eigenvector related to displacement (see Appendix A), and C_{pjqm} being the second-order elastic constants at $\boldsymbol{X}$. Knowing Eqs. (4) and (7), the GGT can be derived in terms of the second- and third-order elastic constants, C^0_{ijmn}

and C^0_{ijmuvn} (see Appendix B for the derivation),

$$\gamma^\beta_{ij}(\boldsymbol{N}) = -\frac{2\Gamma_\beta(\boldsymbol{N})U^\beta_i U^\beta_j + \left(C^0_{ijmn} + C^0_{ijmuvn}U^\beta_u U^\beta_v\right)N_m N_n}{2\Gamma_\beta(\boldsymbol{N})}, \tag{8a}$$

$$\Gamma_\beta(\boldsymbol{N}) = N_i U^\beta_j C^0_{ijkm} U^\beta_k N_m, \tag{8b}$$

with U^β_i being normalized vectors corresponding to polarization.

The TGT can be calculated from the GGT by taking the weighted average of n GGT modes with respect to the heat capacity $C_\beta(\boldsymbol{N}^\xi)$ [4,19]

$$\gamma_{ij} = \frac{\sum_{\xi=1}^{n}\sum_{\beta=1}^{3} C_\beta(\boldsymbol{N}^\xi)\gamma^\beta_{ij}(\boldsymbol{N}^\xi)}{\sum_{\xi=1}^{n}\sum_{\beta=1}^{3} C_\beta(\boldsymbol{N}^\xi)}, \tag{9}$$

with the heat capacity of a given mode being represented as [20]

$$C_\beta(\boldsymbol{N}) = k_B\left(\frac{\hbar\omega_\beta(\boldsymbol{N})}{k_B T}\right)^2 \frac{\exp(\hbar\omega_\beta(\boldsymbol{N})/k_B T)}{[\exp(\hbar\omega_\beta(\boldsymbol{N})/k_B T) - 1]^2}. \tag{10}$$

In the high-temperature limit, the heat capacity becomes constant, which simplifies Eq. (9) to

$$\gamma_{ij} = \frac{1}{3n}\sum_{\xi=1}^{n}\sum_{\beta=1}^{3}\gamma^\beta_{ij}(\boldsymbol{N}^\xi). \tag{11}$$

For the purposes of this study, the heat capacity is approximated using the Debye model, for which the Debye temperature, defined as

$$\Theta_D = \frac{\hbar}{k_B}\left(\frac{6\pi^2}{V_0}\right)^{1/3} W, \tag{12}$$

with V_0 being the atomic volume, is calculated by approximating the crystal to be isotropic. W can be written in terms of the averaged longitudinal and transverse wave velocities (W_L and W_T, respectively) [20] as

$$\frac{3}{W^3} = \frac{1}{W_L^3} + \frac{2}{W_T^3}, \tag{13a}$$

$$\rho_0 W_L^2 = K_{\mathrm{RVH}} + \frac{4}{3}G_{\mathrm{RVH}}, \tag{13b}$$

$$\rho_0 W_T^2 = G_{\mathrm{RVH}}, \tag{13c}$$

with K_{RVH} and G_{RVH} referring to the Reuss-Voigt-Hill average [21] of the bulk modulus and shear modulus.

The effective thermal expansion tensor of a two phase system (α^*_{kl}) can be written as [22]

$$\alpha^*_{kl} = \bar{\alpha}_{kl} + P_{klmn}(S^*_{mnij} - \bar{S}_{mnij})\left(\alpha^{(1)}_{ij} - \alpha^{(2)}_{ij}\right), \tag{14a}$$

$$I_{klrs} = P_{klmn}\left(S^{(1)}_{mnrs} - S^{(2)}_{mnrs}\right), \tag{14b}$$

$$I_{klrs} = \frac{1}{2}(\delta_{kr}\delta_{ls} + \delta_{ks}\delta_{lr}), \tag{14c}$$

where a bar over a quantity denotes the average of the value, superscripts $^{(1)}$ and $^{(2)}$ refer to phase (1) and (2), respectively, and P_{klmn} is defined by Eq. (14b). Equations (14) state that in the case where the elastic constants of the two phases are equal, such as an inclusion in a matrix, the effective thermal expansion tensor of the composite is simply a composition average of the two components.

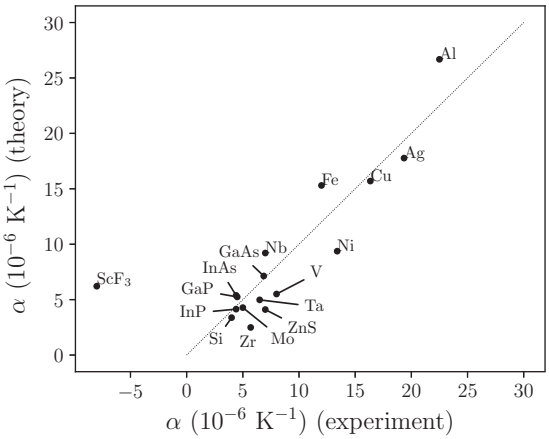

FIG. 1. Benchmarks for coefficients of thermal expansion at 300 K calculated from second and third-order elastic constants of 16 materials. The average mean absolute error relative to the benchmark dataset [30,31] is 1.8×10^{-6} K^{-1} when excluding ScF_3.

III. COMPUTATIONAL DETAILS

The second- and third-order elastic constants were calculated for both the β and α'' phases by applying 21 unique Lagrangian strain states with 9 different magnitudes ranging from $-\eta_{\max}$ (maximum strain) to $\eta_{\max}$, with $\eta_{\max} = 5\%$. This maximum strain was chosen as it caused the trace of the thermal expansion tensor to converge to within 2%. The SOEC and TOEC were determined from the second derivative of the total energy and stress with respect to the strain parameter by means of pseudoinversion. (For a list of the strain components applied as well as a more in depth description of the method, see Ref. [6]). Benchmarking calculations from Fig. 1 use a slightly larger range of strains from −7.5% to 7.5%, and are calculated according to a standard workflow and fitting procedure contained in the ATOMATE [23] and PYMATGEN [24] packages, respectively [25]. It is noted that using a maximum strain of 7.5% for the β and α'' phases gives results in qualitative agreement with the 5% maximum strain results, with the difference in the trace of the thermal expansion tensor being 32% and 13% for the β and α'' phases, respectively. More information on the dependence of thermal expansion on the maximum strain used in the elastic constants calculations is presented in Sec. IV. It should be noted that for all calculations in this work for which SOEC and TOEC were used as inputs, unless otherwise state, the SOEC and TOEC calculated with $\eta_{\max} = 5\%$ were used.

Total energy calculations for both the benchmarks and Ti-Nb calculations were performed using the projector augmented wave method as implemented in the Vienna *ab initio* simulation package [26,27]. The exchange-correlation functional was calculated using the Perdew, Burke, and Ernzerhof generalized gradient approximation [28]. Stress was calculated using the Hellman-Feynman theorem. The elastic constants of the β phase were determined with a $21 \times 21 \times 21$ Γ-centered grid.

TABLE I. Comparison of lattice parameters for β and α'' phases between the current work (CW) with values from literature, both experimental (E) and theoretical (T) for Ti_3Nb. In the case of β the lattice parameter corresponds to $a = (2V_0)^{1/3}$, with V_0 being the volume per atom of the relaxed cell.

Phase	a (Å)	b (Å)	c (Å)
β (CW)	3.25		
β (T) [17]	3.26		
β (E) [15]	3.29		
α'' (CW)	3.34	4.75	4.39
α'' (T) [17]	3.34	4.77	4.41
α'' (E) [15]	3.19	4.80	4.65
α'' (T) [37]	3.30	4.76	4.43

In the case of α'', a $25 \times 17 \times 19$ Γ-centered grid was used. The first-order Methfessel-Paxton smearing scheme [29] was employed with a smearing parameter of 0.05 eV. The total energy was converged to within 1×10^{-10} eV/atom, while ionic relaxations were performed until the magnitudes of all residual forces were less than 5 meV/Å. The plane-wave energy cutoff was set to 600 eV for the α'' and β phases, as all TOEC in the β phase were converged to within 0.5% when compared to using a plane-wave energy cutoff of 700 eV. The benchmark calculations were done using a plane-wave energy cutoff of 700 eV in accordance with the standard elastic constants workflow used by the Materials Project [5].

IV. RESULTS

Benchmarks of thermal expansion coefficients are calculated from the second- and third-order elastic constants of 17 materials (see Fig. 1). We note that these results, which include a variety of cubic and hexagonal materials, agree well with experimental data [30,31] (excluding ScF_3) with an average mean absolute error (MAE) of 1.8×10^{-6} K^{-1}. The agreement is quite good, and suggests that the approach is sound. [The thermal expansion coefficients shown are one-third the trace of the thermal expansion tensor in Eq. (3)].

ScF_3 was included in order to test if the current model can be accurately applied to the class of negative thermal expansion materials containing the $D0_9$ structure [32,33]. The presence and softening of transverse rigid unit modes at the R, X, and M points in the phonon dispersion have been used to explain the anomalous negative thermal expansion of these crystals [34–36]. The failure of our method to accurately predict the thermal expansion of ScF_3 is likely a result of the fact that our model does not directly sample these zone edge phonons that soften locally. This is due to the fact that we only consider the contributions from the long wavelength phonons in our calculation of the TGT and in using the Debye model for the heat capacity.

TABLE III. The second-order elastic constants of β (G1) structure for Ti_3Nb. Units are in GPa.

C^0_{11}	C^0_{12}	C^0_{44}	Reference
148.8	111.4	37.5	[17]
145.2	114.4	36.8	CW ($\eta_{\max} = 5\%$)
151.9	111.1	41.9	CW ($\eta_{\max} = 7.5\%$)

The β phase of gum metal was approximated as the G1 structure described by Lazar *et al.* [17]. This phase was chosen as it was found to exhibit the lowest energy of all possible 16 atom BCC cell configurations with a composition of Ti_3Nb. For the α'' phase, a distorted $L6_0$ structure was found to be most stable [17]. The relaxed unit cells for both phases appear to be in good agreement with both experimental and theoretical calculations of Ti_3Nb as shown in Table I.

In addition to the lattice parameter, it appears that the elastic constants are well reproduced using the pseudoinversion method for both the α'' phase (Table II) as well as β (Table III). This is especially true for β as the difference in values for C^0_{11}, C^0_{12}, and C^0_{44} with the cited reference is 2.42%, 2.69%, and 1.87%, respectively.

While by no means definitive, the agreement between the SOEC of the current work and references is an indicator of the accuracy of the TOEC calculations, which are shown for the two different phases in Tables IV and V. It should be noted that the symmetry of the G1 structure is not cubic. However, in order to approximate G1 as β, the SOEC and TOEC were averaged to be cubic using the relations

$$C^{sym}_{ijkl} = \frac{1}{n_G}\sum_{\alpha=1}^{n_G} a^{(\alpha)}_{ip} a^{(\alpha)}_{jq} a^{(\alpha)}_{kr} a^{(\alpha)}_{ls} C^0_{pqrs}, \tag{15a}$$

$$C^{sym}_{ijklmn} = \frac{1}{n_G}\sum_{\alpha=1}^{n_G} a^{(\alpha)}_{ip} a^{(\alpha)}_{jq} a^{(\alpha)}_{kr} a^{(\alpha)}_{ls} a^{(\alpha)}_{mt} a^{(\alpha)}_{nu} C^0_{pqrstu}, \tag{15b}$$

with $\boldsymbol{a}^{(\alpha)}$ corresponding to the transformation matrix of the α^{th} element of the point group and n_G being the number of elements of the point group. For a BCC system, there are 48 elements of the point group.

To further test the accuracy of the TOEC calculated in this work, the ideal tensile strength was approximated by analyzing the symmetric Wallace tensor as a function of tensile strain [6]. These results were then compared to ideal tensile strength calculations of the G1 structure with a [001] orientation carried out by Nagasako *et al.* [38] that found a shear instability

TABLE II. The second-order elastic constants of α'' Ti_3Nb. Units are in GPa.

C^0_{11}	C^0_{22}	C^0_{33}	C^0_{12}	C^0_{13}	C^0_{23}	C^0_{44}	C^0_{55}	C^0_{66}	Reference
148.1	171.1	174.6	93.0	123.8	80.4	64.7	44.9	32.3	[17]
129.9	148.2	135.6	91.1	126.8	69.3	28.4	23.1	39.7	[37]
141.7	178.3	168.1	94.6	133.3	80.5	47.6	35.1	68.8	CW ($\eta_{\max} = 5\%$)
142.7	179.0	172.8	94.9	130.2	79.8	47.0	35.0	68.1	CW ($\eta_{\max} = 7.5\%$)

TABLE IV. The symmetrized third-order elastic constants of β (G1) structure for Ti_3Nb. Units are in GPa.

η_{max}	C^0_{111}	C^0_{112}	C^0_{123}	C^0_{144}	C^0_{166}	C^0_{456}
5%	−1207	−542.5	246.0	−256.3	−169.2	189.0
7.5%	−1226	−402.9	−97.6	−309.6	−136.6	173.5

associated with $C_{11} - C_{12} \to 0$ to occur at approximately 6% strain and at a stress of 2.5 GPa. In comparison, this work's ideal tensile strength calculations find the same shear instability to occur at 5.5% strain (see Fig. 2) corresponding to an ideal tensile strength of 2.89 GPa. This supports using TOEC to describe the elastic anharmonicity of Ti_3Nb.

Using SOEC and TOEC, the thermodynamic Grüneisen tensor as well as the thermal expansion tensor have been calculated for both β and α'' approximants. Both Eqs. (9) and (11) were used to determine γ_{ij} with no difference in the two averaging methods to the accuracy shown in Table VI. In calculating the heat capacity a temperature of 300 K was used. As the Debye temperature for both phases is near room temperature (Table VI), this helps explain the correspondence between the two averaging schemes.

The linear expansion coefficient of the β phase compares quite well with experimental values. Saito *et al.* measured a value of 8×10^{-6} K^{-1} for annealed gum metal [9] while Kim *et al.* found a value of 7.2×10^{-6} K^{-1} [15]. The negative components of the thermal expansion tensor for α'' appear to support the claim made by Kim *et al.* that the Invar properties of gum metal are the result of a texturing effect as α_{22} and α_{33} for the orthorhombic phase correspond to ⟨110⟩ directions in the β phase [15].

Work by Kim *et al.* [15] as well as Morris *et al.* [39] found that cold-rolling gum metal caused a ⟨110⟩ texturing in the RD and no such dramatic texturing in the TD. This corresponded

TABLE V. Third-order elastic constants of α'' structure for Ti_3Nb. Units are in GPa. Elastic constants are presented for calculations using $\eta_{max} = 5\%$ and 7.5%.

		$\eta_{max} = 5\%$		
C^0_{111}	C^0_{222}	C^0_{333}	C^0_{112}	C^0_{122}
−1402	−1599	−882.0	−166.6	−447.2
C^0_{113}	C^0_{133}	C^0_{223}	C^0_{233}	C^0_{123}
−367.8	−684.0	−187.2	−418.4	−171.8
C^0_{144}	C^0_{155}	C^0_{166}	C^0_{244}	C^0_{255}
101.9	−282.3	−334.4	−161.9	−94.0
C^0_{266}	C^0_{344}	C^0_{355}	C^0_{366}	C^0_{456}
−240.5	−286.6	−131.0	−195.1	−14.90
		$\eta_{max} = 7.5\%$		
C^0_{111}	C^0_{222}	C^0_{333}	C^0_{112}	C^0_{122}
−1535	−1163	−967.9	−84.47	−579.6
C^0_{113}	C^0_{133}	C^0_{223}	C^0_{233}	C^0_{123}
−310.1	−662.5	−317.0	−395.2	−147.7
C^0_{144}	C^0_{155}	C^0_{166}	C^0_{244}	C^0_{255}
111.7	−269.0	−316.4	−235.5	−147.7
C^0_{266}	C^0_{344}	C^0_{355}	C^0_{366}	C^0_{456}
−280.9	−301.3	−169.2	−182.3	−2.925

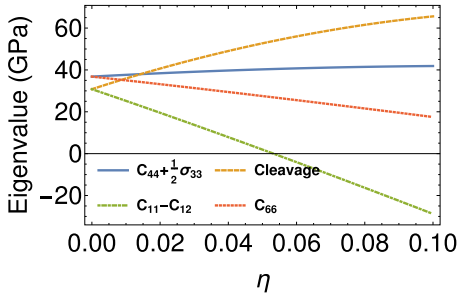

FIG. 2. The eigenvalues of the symmetric Wallace tensor plotted as a function of the Lagrangian strain, η, for a uniaxial load applied in the [001] direction. Three of the modes correspond to shear $[\frac{1}{2}(C_{11} - C_{12}), C_{66}$, and $C_{44} + \frac{1}{2}\sigma_{33}]$ while failure in cleavage corresponds to brittle fracture. Failure occurs at a strain of 5.5% and a stress of 2.89 GPa.

to a RD thermal expansion coefficient of -0.7×10^{-6} K^{-1} and no change in the thermal expansion coefficient in the TD compared to the single-crystal sample. If we assume that the elastic constants of α'' and β phases are the same, then we can approximate the thermal expansion tensor using the rule of mixing. Assuming that the thermal expansion coefficient in the RD of α'' is $\alpha_{RD}(\alpha'') = \frac{\alpha_{22}(\alpha'')+\alpha_{33}(\alpha'')}{2}$ and that the thermal expansion of α'' in the TD is isotropic, $\alpha_{TD}(\alpha'') = \alpha_{kk}(\alpha'')/3$, at a volume fraction of 0.172 α'' the RD and TD thermal expansion coefficients of the composites are $\alpha^C_{RD} = -0.7 \times 10^{-6}$ K^{-1} and $\alpha^C_{TD} = 6.5 \times 10^{-6}$ K^{-1}, respectively. The volume fraction of α'' seems plausible as high-energy x-ray diffuse scattering studies of the deformation of Ti-24Nb-4Zr-8Sn-0.10O (wt %), an alloy with a composition similar to gum metal's, show a volume fraction of the martensitic phase to be between 0 and 0.4 while still in the elastic regime [14].

To test the assumption that the thermal expansion coefficient of the composite can be approximated as the weighted average of the two different phases, the effective thermal expansion tensor of a homogeneous mixture of the β and α'' phases was calculated using Voigt-Reuss bounds on the elastic constants. In the case of the Reuss average $S^*_{ijkl} = \bar{S}_{ijkl}$, resulting in $\alpha^*_{ij} = \bar{\alpha}_{ij}$. For the Voigt average, isotropic elastic constants, (G_V and K_V) were calculated for both phases and then averaged by composition. Using Eq. (14) the effective thermal expansion tensor was calculated as a function of α'' composition. The results of this comparison can be seen in Fig. 3. The maximum

TABLE VI. Thermodynamic quantities derived from the elastic constants including the nonzero components of the thermodynamic Grüneisen tensor, the Debye temperature (K), and the thermal expansion tensor (1×10^{-6} K^{-1}). The results for α_{ij} are at 300 K. Results for TOEC calculated using a maximum strain of 5% and 7.5% strain are displayed.

Phase	γ_{11}	γ_{22}	γ_{33}	Θ_D	α_{11}	α_{22}	α_{33}
β (5%)	1.25	1.25	1.25	278	8.59	8.59	8.59
β (7.5%)	0.95	0.95	0.95	282	5.81	5.81	5.81
α'' (5%)	0.99	0.65	0.08	319	60.9	−3.46	−45.6
α'' (7.5%)	1.10	0.59	0.34	327	45.2	−4.26	−27.6

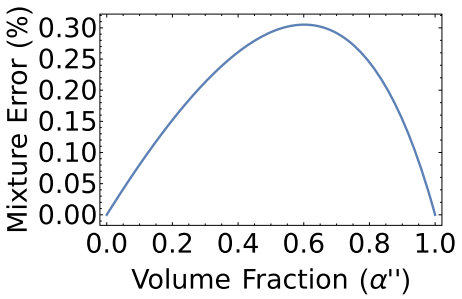

FIG. 3. Measure of error as a function of volume fraction between a mixture average (Reuss average), $\bar{\alpha}(x) = (1-x)\alpha_\beta + x\alpha_{\rm iso}^{\alpha''}$, with x being the volume fraction of α'', and the Voigt average of the thermal expansion using equation (14). The error is defined as $e_{\rm mix} = \frac{|\bar{\alpha}-\alpha^*|}{\alpha^*}$. It should be noted that the isotropic thermal expansion coefficient is approximated for the α'' phase and has the form $\alpha_{\rm iso}^{\alpha''} = \frac{1}{3}\alpha_{\rm kk}^{\alpha''}$.

error occurs at an α'' volume fraction of approximately 60% and amounts to an error of only 0.30%. This small error is a strong indicator that the rule of mixing is accurate in describing the thermal expansion of the two phase system.

V. DISCUSSION

The benchmark calculations of the thermal expansion coefficient shown in Fig. 1 demonstrate that the method described in this paper is capable of accurately predicting the thermal expansion tensor for a range of crystalline materials. This offers the possibility of a framework to perform accurate high-throughput calculations of the thermal expansion coefficient with a caveat. As the thermal expansion is dependent on heat capacity, which is approximated using the Debye model, one can only use this method for materials at temperatures under which the Debye model applies. A notable class of materials where this approximation is not accurate are the $D0_9$-type crystals (e.g., ReO_3 and ScF_3) [32,33] that display noticeable negative thermal expansion over a wide range of temperatures. Negative thermal expansion in these materials is attributed to transverse rigid unit modes at the R, X, or M point in the phonon dispersion [34–36], which would not be directly sampled by the approach applied within this work. The accuracy of these benchmark calculations provides support, however, for applying the method discussed in this paper to more complex systems than elemental metals, such as the two-phase approximation of gum metal.

As the two phases of gum metal in question do not contain any off-diagonal components in the thermal expansion tensor, from Eq. (14), it can be seen that no shear components of the compliance tensor effect the effective thermal expansion coefficient. Calculating the Voigt bulk modulus, $K_V^{\rm cubic} = \frac{C_{11}^0+2C_{12}^0}{3}$ and $K_V^{\rm ortho} = \frac{C_{11}^0+C_{22}^0+C_{33}^0+2(C_{12}^0+C_{13}^0+C_{23}^0)}{9}$, the bulk moduli come to 125 and 123 GPa for the cubic and orthorhombic phases, respectively, while the Reuss average of the orthorhombic phase is 122 GPa (the Voigt and Reuss averages are equal for a cubic system). Considering that the Voigt-Reuss bounds have been shown to be the upper and lower bounds on the elastic modulus of a composite material [21], using stricter bounds for the orthorhombic phase (such as Hashin-Shtrikman [40,41]) would not result in dramatically different bulk moduli.

The TGT for the α'' phase is positive, but near zero for γ_{22} and γ_{33}, while γ_{11} is near that of the β phase. The high anisotropy of the TGT coupled with S_{12} and S_{13} being negative results in a negative value for α_{22} and α_{33}. The fact that the α'' phase is calculated to show negative thermal expansion in the $\langle 110\rangle_\beta$ direction supports earlier experimental results that found the Invar properties of gum metal to be the result of a martensitic phase transformation. Furthermore, the fact that the high anisotropy of the thermodynamic Grüneisen tensor leads to negative components in the thermal expansion tensor suggests Invar properties of gum metal could be a direct result of the breaking of cubic symmetry.

This work demonstrates that the formation of the α'' phase can lead to Invar behavior in gum metal. However, an interesting question that arises is what effect, if any, the softening of the $\Gamma - N$ phonon branch within the β phase has on the thermal expansion of gum metal. This phonon is involved in the BCC-HCP transformation [42], on which the α'' phase can be seen as an intermediate structure. Hanlumyuang *et al.* [43] demonstrated that a softening of the Γ-N phonons could lead to diffuse scattering, resulting in a diffraction pattern similar to that in which the α'' phase was present. Perhaps it is possible for gum metal to achieve Invar behavior without the formation of a cubic symmetry breaking secondary phase due to the softening of the Γ-N phonon branch softening.

VI. CONCLUSION

A framework for efficiently estimating the thermal expansion tensor of a crystal has been detailed. Comparison of the results of this method to experimental values of the thermal expansion coefficient demonstrates the high accuracy of this simple model. In addition, this approach has been applied in order to understand the origin of the Invar behavior observed in gum metal. The thermal expansion tensor for both the β and α'' phases were calculated by relating the thermal expansion tensor to the second- and third-order elastic constants of Ti_3Nb gum metal approximants of the two phases. Ideal strength calculations using the elastic constants produced results in line with prior work on the ideal tensile behavior of the G1 structure of Ti_3Nb.

The thermal expansion of the β phase of gum metal appears to be well approximated by the G1 structure. In agreement with experimental studies, the α'' phase is shown to have a negative thermal expansion along $\langle 110\rangle_\beta$. It is shown that the rule of mixing is a simple and accurate approach for estimating the thermal expansion tensor of the two phase system. This allows for estimations of the α'' concentration needed to reproduce experimental findings on the thermal expansion of gum metal after cold-rolling. The findings of this paper indicate that the formation of the α'' phase could be the origin of the Invar-like behavior of gum metal, which would parallel the behavior of known nonmagnetic Invar materials such as Al-Cu-Zn and other shape-memory alloys, but it does not nullify completely the idea that gum metal's thermal expansion behavior is a direct result of the softening of the N-point phonon.

ACKNOWLEDGMENTS

The authors acknowledge Maarten de Jong for insightful discussions. This work was funded by the U.S. Department of

Energy, Office of Science, Office of Basic Energy Sciences, Materials Sciences and Engineering Division under Contract No. DE-AC02-05-CH11231 (Materials Project program KC23MP).

APPENDIX A: DERIVATION OF CHRISTOFFEL EQUATION

In arriving at Eq. (7), it is helpful to approximate the first Piola-Kirchhoff stress tensor as a Taylor series expansion to the first order centered at $\boldsymbol{X}$, of the form

$$\tilde{P}_{jp} \approx P_{jp} + \left[\frac{\partial \tilde{P}_{jp}}{\partial \tilde{F}_{km}}\right]_{\tilde{\boldsymbol{F}}=\boldsymbol{F}} (\tilde{F}_{km} - F_{km}), \tag{A1a}$$

$$\tilde{F}_{km} = \frac{\partial x_k}{\partial a_m}, \tag{A1b}$$

$$F_{km} = \frac{\partial X_k}{\partial a_m}, \tag{A1c}$$

with P_{jp} representing the first Piola-Kirchhoff stress tensor at $\boldsymbol{X}$. To find the right-hand side of Eq. (6) one can take the derivative of the Taylor series with respect to $\boldsymbol{a}$, which gives

$$\frac{\partial \tilde{P}_{jp}}{\partial a_p} \approx \left[\frac{\partial \tilde{P}_{jp}}{\partial \tilde{F}_{km}}\right]_{\tilde{\boldsymbol{F}}=\boldsymbol{F}} \frac{\partial^2 u_k}{\partial a_m \partial a_p}. \tag{A2}$$

By substituting (5) into (A2), the equation of motion is now of the form

$$\rho_0 W^2 u_j = \left[\frac{\partial \tilde{P}_{jp}}{\partial \tilde{F}_{km}}\right]_{\tilde{\boldsymbol{F}}=\boldsymbol{F}} N_m N_p u_k. \tag{A3}$$

$\frac{\partial \tilde{P}_{jp}}{\partial \tilde{F}_{km}}$ can be further evaluated by taking into account that $\tilde{P}_{jp} = \tilde{F}_{jq}\tilde{t}_{pq}$, $\tilde{t}_{pq}$ being the second Piola-Kirchhoff stress tensor. Using this relation the chain rule can be applied to express $\frac{\partial \tilde{P}_{jp}}{\partial \tilde{F}_{km}}$ as

$$\frac{\partial \tilde{P}_{jp}}{\partial \tilde{F}_{km}} = \frac{\partial}{\partial \tilde{F}_{km}}(\tilde{F}_{jq}\tilde{t}_{pq}), \tag{A4a}$$

$$\frac{\partial \tilde{P}_{jp}}{\partial \tilde{F}_{km}} = \delta_{jk}\tilde{t}_{pm} + \tilde{F}_{jq}\frac{\partial \tilde{t}_{pq}}{\partial \tilde{\eta}_{st}}\frac{\partial \tilde{\eta}_{st}}{\partial \tilde{F}_{km}}. \tag{A4b}$$

with $\tilde{\eta}_{st}$ being the Lagrangian strain relating $\boldsymbol{x}$ and $\boldsymbol{a}$. As the Lagrangian strain is related to the deformation gradient by $\tilde{\eta}_{ij} = \frac{1}{2}(\tilde{F}_{ki}\tilde{F}_{kj} - \delta_{ij})$ (A4) can be written as

$$\frac{\partial \tilde{P}_{jp}}{\partial \tilde{F}_{km}} = \delta_{jk}\tilde{t}_{pm} + \tilde{F}_{jq}\tilde{F}_{kt}\tilde{C}_{pqmt}, \tag{A5}$$

where $\tilde{\boldsymbol{C}}$ are the elastic constants in configuration $\boldsymbol{x}$ and obey Voigt symmetry. Substituting (A5) into (A3) results in

$$\rho_0 W^2 u_j = (\delta_{jk}t_{pm} + F_{jq}F_{kt}C_{pqmt})N_m N_p u_k, \tag{A6}$$

with $\boldsymbol{t}$ and $\boldsymbol{C}$ being the second Piola-Kirchhoff stress tensor and elastic constants in the configuration $\boldsymbol{X}$. Finally, it is helpful to write the displacement with respect to the reference configuration as $u_j = F_{js}U_s$. Applying this relation to (A6) gives

$$\rho_0 W^2 U_r = (\delta_{rs}t_{pm} + F_{kt}F_{ks}C_{prmt})N_m N_p U_s. \tag{A7}$$

Because of the definition of the Lagrangian strain, the term $F_{kt}F_{ks} = 2\eta_{ts} + \delta_{ts}$, which results in (7).

APPENDIX B: DERIVATIVE OF $\rho_0 W^2$ WITH RESPECT TO STRAIN

In applying the Debye model, the phonon frequency of a particular mode, $\omega_p(\boldsymbol{q})$ is proportional to the unstrained wave speed

$$\omega_p(\boldsymbol{q}) \propto W_p(\boldsymbol{N})/L_0, \tag{B1}$$

with L_0 being the dimension of the unstrained crystal. Substituting (B1) into the definition of the GGT (4) yields

$$\gamma_{ij}^{\beta}(\boldsymbol{N}) = -\frac{1}{W_\beta(\boldsymbol{N})}\left[\frac{\partial W_\beta(\boldsymbol{N})}{\partial \eta_{ij}}\right]_{\boldsymbol{\eta}'}. \tag{B2}$$

Using the relation

$$\frac{\partial}{\partial \eta_{jk}}(W_\beta(\boldsymbol{N})^2) = 2W_\beta(\boldsymbol{N})\frac{\partial W_\beta(\boldsymbol{N})}{\partial \eta_{jk}}, \tag{B3}$$

the GGT can be rewritten as

$$\gamma_{ij}^{\beta}(\boldsymbol{N}) = -\frac{1}{2\rho_0 W_\beta(\boldsymbol{N})^2}\left[\frac{\partial(\rho_0 W_\beta(\boldsymbol{N})^2)}{\partial \eta_{ij}}\right]_{\boldsymbol{\eta}'}. \tag{B4}$$

The above equation can be further evaluated with the help of (7). To obtain $[\frac{\partial(\rho_0 W_\beta(\boldsymbol{N})^2)}{\partial \eta_{pq}}]_{\boldsymbol{\eta}'}$, one can differentiate both sides of equation (7) by η_{pq}. This results in

$$\frac{\partial}{\partial \eta_{pq}}(\rho_0 W^2)U_j + \rho_0 W^2 \frac{\partial U_j}{\partial \eta_{pq}} = \frac{\partial \Gamma_{jk}}{\partial \eta_{pq}}U_k + \Gamma_{jk}\frac{\partial U_k}{\partial \eta_{pq}}. \tag{B5}$$

Since $\boldsymbol{U}$ is a unit vector ($U_j U_j = 1$), meaning that $U_j \frac{\partial U_j}{\partial \eta_{pq}} = 0$. If each side of equation (B5) is dotted with U_j this yields

$$\frac{\partial}{\partial \eta_{pq}}(\rho_0 W^2) = U_j \frac{\partial \Gamma_{jk}}{\partial \eta_{pq}}U_k + U_j \Gamma_{jk}\frac{\partial U_k}{\partial \eta_{pq}}. \tag{B6}$$

Due to the symmetry inherent to the elastic tensor, $\boldsymbol{\Gamma}$ is symmetric ($\Gamma_{jk} = \Gamma_{kj}$). By rewriting Eq. (7a) as $\rho_0 W^2 U_j = \Gamma_{jk}U_k$, the second term in Eq. (B6) becomes

$$U_j \Gamma_{jk}\frac{\partial U_k}{\partial \eta_{pq}} = \rho_0 W^2 U_k \frac{\partial U_k}{\partial \eta_{pq}}, \tag{B7}$$

which must be equal to zero. This leaves

$$\frac{\partial}{\partial \eta_{pq}}(\rho_0 W^2) = U_j \frac{\partial \Gamma_{jk}}{\partial \eta_{pq}}U_k. \tag{B8}$$

If Eq. (7b) is combined with (B4) and (B8) and evaluated at $\boldsymbol{\eta} = \boldsymbol{0}$ one is left with Eq. (8).

[1] N. W. Ashcroft and N. D. Mermin, *Solid State Physics* (Holt, Rinehart and Winston, 1976).

[2] K. Brugger, Phys. Rev. **137**, A1826 (1965).

[3] R. N. Thurston and K. Brugger, Phys. Rev. **133**, A1604 (1964).

[4] Y. Hiki, J. F. Thomas, and A. V. Granato, Phys. Rev. **153**, 764 (1967).

[5] M. De Jong, W. Chen, T. Angsten, A. Jain, R. Notestine, A. Gamst, M. Sluiter, C. K. Ande, S. Van Der Zwaag, J. J. Plata *et al.*, Sci. Data **2**, 150009 (2015).

[6] M. de Jong, I. Winter, D. C. Chrzan, and M. Asta, Phys. Rev. B **96**, 014105 (2017).

[7] C. E. Guillaume, Proc. Phys. Soc. London **32**, 374 (1919).

[8] R. Kainuma, J. Wang, T. Omori, Y. Sutou, and K. Ishida, Appl. Phys. Lett. **80**, 4348 (2002).

[9] T. Saito, T. Furuta, J.-H. Hwang, S. Kuramoto, K. Nishino, N. Suzuki, R. Chen, A. Yamada, K. Ito, Y. Seno *et al.*, Science **300**, 464 (2003).

[10] T. Li, J. W. Morris, N. Nagasako, S. Kuramoto, and D. C. Chrzan, Phys. Rev. Lett. **98**, 105503 (2007).

[11] D. C. Chrzan, J. W. Morris, Y. N. Osetsky, R. E. Stoller, and S. J. Zinkle, MRS Bull. **34**, 173 (2009).

[12] R. Talling, R. Dashwood, M. Jackson, and D. Dye, Acta Mater. **57**, 1188 (2009).

[13] E. A. Withey, A. M. Minor, D. C. Chrzan, J. W. Morris, Jr., and S. Kuramoto, Acta Mater. **58**, 2652 (2010).

[14] J.-P. Liu, Y.-D. Wang, Y.-L. Hao, Y. Wang, Z.-H. Nie, D. Wang, Y. Ren, Z.-P. Lu, J. Wang, H. Wang *et al.*, Sci. Rep. **3**, 2156 (2013).

[15] H. Y. Kim, L. Wei, S. Kobayashi, M. Tahara, and S. Miyazaki, Acta Mater. **61**, 4874 (2013).

[16] P. Souvatzis, O. Eriksson, and M. I. Katsnelson, Phys. Rev. Lett. **99**, 015901 (2007).

[17] P. Lazar, M. Jahnátek, J. Hafner, N. Nagasako, R. Asahi, C. Blaas-Schenner, M. Stöhr, and R. Podloucky, Phys. Rev. B **84**, 054202 (2011).

[18] D. C. Wallace, *Thermodynamics of Crystals* (Courier Corporation, 1998).

[19] T. Barron, Phil. Mag. J. Sci. **46**, 720 (1955).

[20] G. Grimvall, *Thermophysical Properties of Materials* (Elsevier, 1999) pp. 70–86,116–118.

[21] R. Hill, Proc. Phys. Soc. London, Sec. A **65**, 349 (1952).

[22] B. W. Rosen and Z. Hashin, Int. J. Eng. Sci. **8**, 157 (1970).

[23] K. Mathew, J. H. Montoya, A. Faghaninia, S. Dwarakanath, M. Aykol, H. Tang, I. heng Chu, T. Smidt, B. Bocklund, M. Horton, J. Dagdelen, B. Wood, Z.-K. Liu, J. Neaton, S. P. Ong, K. Persson, and A. Jain, Comput. Mater. Sci. **139**, 140 (2017).

[24] S. P. Ong, W. D. Richards, A. Jain, G. Hautier, M. Kocher, S. Cholia, D. Gunter, V. L. Chevrier, K. A. Persson, and G. Ceder, Comput. Mater. Sci. **68**, 314 (2013).

[25] A standard high-throughput methodology for the calculation of higher-order elastic constants will be the subject of a forthcoming publication.

[26] G. Kresse and J. Furthmüller, Phys. Rev. B **54**, 11169 (1996).

[27] G. Kresse and J. Hafner, Phys. Rev. B **47**, 558 (1993).

[28] J. P. Perdew, K. Burke, and M. Ernzerhof, Phys. Rev. Lett. **77**, 3865 (1996).

[29] M. Methfessel and A. T. Paxton, Phys. Rev. B **40**, 3616 (1989).

[30] *ASM Ready Reference. Thermal Properties of Metals*, edited by F. Cverna (Materials Park, Ohio : ASM International, 2002).

[31] L. B. Freund and S. Suresh, *Thin Film Materials: Stress, Defect Formation and Surface Evolution* (Cambridge University Press, 2004).

[32] G. D. Barrera, J. A. O. Bruno, T. H. K. Barron, and N. L. Allan, J. Phys.: Condens. Matter **17**, R217(R) (2005).

[33] B. K. Greve, K. L. Martin, P. L. Lee, P. J. Chupas, K. W. Chapman, and A. P. Wilkinson, J. Am. Chem. Soc. **132**, 15496 (2010).

[34] C. W. Li, X. Tang, J. A. Muñoz, J. B. Keith, S. J. Tracy, D. L. Abernathy, and B. Fultz, Phys. Rev. Lett. **107**, 195504 (2011).

[35] U. D. Wdowik, K. Parlinski, T. Chatterji, S. Rols, and H. Schober, Phys. Rev. B **82**, 104301 (2010).

[36] P. Lazar, T. Bučko, and J. Hafner, Phys. Rev. B **92**, 224302 (2015).

[37] J. Sun, Q. Yao, H. Xing, and W. Guo, J. Phys.: Condens. Matter **19**, 486215 (2007).

[38] N. Nagasako, R. Asahi, and J. Hafner, Phys. Rev. B **85**, 024122 (2012).

[39] J. W. Morris, Jr., Y. Hanlumyuang, M. Sherburne, E. Withey, D. C. Chrzan, S. Kuramoto, Y. Hayashi, and M. Hara, Acta Mater. **58**, 3271 (2010).

[40] J. Willis, J. Mech. Phys. Solids **25**, 185 (1977).

[41] J. P. Watt, J. Appl. Phys. **50**, 6290 (1979).

[42] W. Burgers, Physica **1**, 561 (1934).

[43] Y. Hanlumyuang, R. P. Sankaran, M. P. Sherburne, J. W. Morris, and D. C. Chrzan, Phys. Rev. B **85**, 144108 (2012).